



Contents lists available at ScienceDirect

Journal of the Mechanical Behavior of Biomedical Materials

journal homepage: www.elsevier.com/locate/jmbbm

The relationship between thiol-acrylate photopolymerization kinetics and hydrogel mechanics: An improved model incorporating photobleaching and thiol-Michael addition

Hongyuan Zhu^{a,b}, Xiaoxiao Yang^{a,b}, Guy M. Genin^{a,b,c,d}, Tian Jian Lu^{e,f}, Feng Xu^{a,b}, Min Lin^{a,b,*}

^a The Key Laboratory of Biomedical Information Engineering of Ministry of Education, School of Life Science and Technology, Xi'an Jiaotong University, Xi'an 710049, PR China

^b Bioinspired Engineering & Biomechanics Center (BEBC), Xi'an Jiaotong University, Xi'an 710049, PR China

^c Department of Mechanical Engineering & Materials Science, Washington University in St. Louis, St. Louis 63130, MO, USA

^d NSF Science and Technology Center for Engineering Mechanobiology, Washington University in St. Louis, St. Louis 63130, MO, USA

^e State Key Laboratory of Mechanics and Control of Mechanical Structures, Nanjing University of Aeronautics and Astronautics, Nanjing 210016, PR China

^f MOE Key Laboratory for Multifunctional Materials and Structures, Xi'an Jiaotong University, Xi'an 710049, PR China

ARTICLE INFO

Keywords:

Elastic modulus

Hydrogels

Thiol-acrylate polymerization

Eosin Y

Thiol-Michael addition

ABSTRACT

Biocompatible hydrogels with defined mechanical properties are critical to tissue engineering and regenerative medicine. Thiol-acrylate photopolymerized hydrogels have attracted special interest for their degradability and cytocompatibility, and for their tunable mechanical properties through controlling factors that affect reaction kinetics (e.g., photopolymerization, stoichiometry, temperature, and solvent choice). In this study, we hypothesized that the mechanical property of these hydrogels can be tuned by photoinitiators via photobleaching and by thiol-Michael addition reactions. To test this hypothesis, a multiscale mathematical model incorporating both photobleaching and thiol-Michael addition reactions was developed and validated. After validating the model, the effects of thiol concentration, light intensity, and pH values on hydrogel mechanics were investigated. Results revealed that hydrogel stiffness (i) was maximized at a light intensity-specific optimal concentration of thiol groups; (ii) increased with decreasing pH when synthesis occurred at low light intensity; and (iii) increased with decreasing light intensity when synthesis occurred at fixed precursor composition. The multiscale model revealed that the latter was due to higher initiation efficiency at lower light intensity. More broadly, the model provides a framework for predicting mechanical properties of hydrogels based upon the controllable kinetics of thiol-acrylate photopolymerization.

1. Introduction

Thiol-ene photopolymerizations provide a powerful tool for the design of hydrogels with excellent tunability, degradability, and cytocompatibility (Brown and Anseth, 2017; Ruskowitz and DeForest, 2018; Yao et al., 2018). Most thiol-ene photopolymerizations proceed via a step-growth technique, while thiol-acrylate photopolymerization can proceed by a combination of step-growth and chain-growth techniques that can enhance chemical and mechanical properties (Hoyle and Bowman, 2010; Lee et al., 2007). Hydrogels formed by thiol-acrylate photopolymerization have thus found widespread applications in tissue engineering and regenerative medicine (Chung et al., 2016; Fu et al., 2015; Greene et al., 2017; Hao and Lin, 2014; Hao et al., 2014; Higham

et al., 2014; Lin et al., 2015). For these applications, it is of great importance to understand and predict hydrogel mechanics as a function of synthesis conditions (Cheng et al., 2017; Han et al., 2016; Huang et al., 2017; Sadtler et al., 2016).

The mechanics of hydrogels formed by thiol-acrylate photopolymerization are determined by many factors, such as light intensity (Fu et al., 2015; Hao and Lin, 2014; Lin et al., 2015; Ulasan et al., 2015); molecular weight, stoichiometry and functionalities of monomers (Fu et al., 2015; Greene et al., 2017; Hao and Lin, 2014; Reddy et al., 2006; Ulasan et al., 2015); and chemical properties and concentration of initiators (Greene et al., 2017; Hao and Lin, 2014). Understanding the effects of these variables on reaction kinetics and the emergent mechanics of hydrogels is now typically achieved via

* Corresponding author at: The Key Laboratory of Biomedical Information Engineering of Ministry of Education, School of Life Science and Technology, Xi'an Jiaotong University, Xi'an 710049, PR China.

E-mail address: minlin@mail.xjtu.edu.cn (M. Lin).

<https://doi.org/10.1016/j.jmbbm.2018.08.013>

Received 9 February 2018; Received in revised form 21 July 2018; Accepted 17 August 2018

Available online 24 August 2018

1751-6161/ © 2018 Elsevier Ltd. All rights reserved.

intensive experimental studies, which is time-consuming. There is therefore a pressing need for models to predict how reaction kinetics at the nano- to microscale relates to mechanics at the centimeter-level macroscale.

Thus, considerable effort has been devoted to theoretical modeling of photopolymerization process. The kinetic models of Bowman et al. for various thiol-ene photopolymerizations establish the effects of stoichiometry and numbers of monomer functional groups on the kinetics and subsequent mechanics of hydrogels formed by these reactions (Cramer and Bowman, 2001; Cramer et al., 2003; Lee et al., 2007; Reddy et al., 2006). The multidimensional population balance models of Iedema et al. can be used to relate details of photopolymerization to hydrogel mechanics (Iedema et al., 2018; Kryven and Iedema, 2013, 2014a, 2014b, 2015; Schamboeck et al., 2017). However, photochemical properties of initiators and possible anion mediated side reaction are poorly understood in existing models for thiol-ene photopolymerizations, which limit the applicable conditions and prediction accuracy of these model.

Eosin Y can initiate photopolymerization by photo-induced reductive electron transfer from chain transfer agents (e.g., amines and thiols (Greene et al., 2017; Hao and Lin, 2014; Hao et al., 2014; Lin et al., 2015; Shih and Lin, 2013)); however, the kinetics of Eosin Y in photopolymerization has not yet been modeled. The concentration of eosin Y was simply considered to decline exponentially with a fixed time constant in previous models (Kizilel et al., 2006; Wong et al., 2015). This simplification cannot accurately depict the complex photochemical properties of eosin Y over the range of polymerization conditions because the consumption of eosin Y through photobleaching is sensitive to initial reaction conditions and stoichiometry. This photobleaching occurs due to production of leuco-products by photo-induced reductive electron transfer (Dadashi-Silab et al., 2016; Gorner, 2008; Herculano et al., 2013; Popielarz and Vogt, 2008). However, the complex photo-chemical properties of eosin Y remain elusive.

Polymerization in thiol-acrylate systems proceeds not only via the free radical pathway as mentioned above, but also by an anion pathway (i.e., thiol-Michael addition) (Liu et al., 2014; Marklein and Burdick, 2010; Nair et al., 2014). Michael addition is a reaction paradigm characterized as enolate-type nucleophile reaction, which includes various reaction types such as carbon-Michael addition, oxa-Michael addition, aza-Michael addition and thiol-Michael addition (Nair et al., 2014). Due to its inherent electron density of the S atom, thiol-Michael addition could co-exist in mild aqueous condition with photopolymerization, which has been utilized to design step crosslinkable hydrogels (Marklein and Burdick, 2010; Rape et al., 2015). Unlike the radical mediated thiol-acrylate reaction, thiol-Michael addition between thiols and acrylates is purely step-growth mechanism that proceeds spontaneously in the absence of light excitation (Claudino et al., 2016). The rate of thiol-Michael addition is relatively slow in neutral solution compared to that of photopolymerization for a range of light intensity that is typically on the order of 10–100 mW cm⁻². Thus, thiol-Michael addition is often neglected in modeling study of thiol-acrylate reactions (Claudino et al., 2016; Higham et al., 2014; Huang et al., 2017; Iedema et al., 2018; Liu et al., 2014; Marklein and Burdick, 2010; Nair et al., 2014; Reddy et al., 2006). However, when the light intensity is low (e.g., below 10 mW cm⁻²) and photopolymerization occurs in an alkaline solution, the rates for photopolymerization and thiol-Michael addition are comparable. Although theoretical models exist for pure thiol-Michael addition of thiol-vinyl sulfone (Claudino et al., 2016), they have not considered the possible competition between thiol-Michael addition and photopolymerization.

In this work, a network model is established to investigate the role of photobleaching and thiol-Michael addition in thiol-acrylate photopolymerization, which is then verified against experimental results. Based on the verified model, the development and elasticity of polymer networks formed by thiol-acrylate photopolymerization are predicted under different thiol concentrations, light intensities, and pH values.

These modeling results provide mechanistic insights into relationship between these three factors and the final elasticity of polymer network.

2. Materials and methods

2.1. Experiment methods

2.1.1. Materials

Poly(ethylene glycol) dimethacrylate (PEGDMA, $M_n \approx 1000 \text{ g mol}^{-1}$), dithiothreitol (DTT), eosin Y disodium salt, mono-basic potassium phosphate (KH₂PO₄, 99%) and sodium phosphate dibasic dodecahydrate (Na₂HPO₄·12H₂O, 99%) were purchased from Sigma-Aldrich.

2.1.2. Sample preparation

The polymerization was initiated using light-emitting diodes (LEDs) with emission peak centered at 520 nm. The light intensity was set to be 100 mW/cm². The concentration of photo-initiator eosin Y was 0.1 mmol L⁻¹ for each sample. The concentration of PEGDMA was 0.2 mol L⁻¹ for each sample. The pH value of samples was adjusted by two phosphates (KH₂PO₄/Na₂HPO₄), which was around 6.8 for neutral solution and 8.3 for alkaline solution. A volume of 200 μL of each hydrogel precursor was added on a Teflon plate, and was then covered by a cleaned 2 × 2 cm coverslips to form a gel with 0.5 mm height. All reactions were done under atmospheric conditions.

2.1.3. UV-vis absorption measurements

100 μL precursor solutions at different reaction time (from 0 to 4 min) were collected from the Teflon plate, and were then diluted into 400 μL DI water. Absorption spectra (400–600 nm) of the polymer diluent were recorded on a UV-3600 UV-Vis-NIR absorption spectrophotometer at room temperature.

2.1.4. ¹HNMR spectrum measurements

Hydrogel precursors were dissolved into D₂O. All samples were obtained by irradiating polymer precursors with green LED at intensity of 100 mW/cm² for 16 min before the tests. The gels were crushed and suspended in D₂O. The monomer conversion was determined by ¹HNMR spectroscopy (Bruker Advance III HD 400M) of the crude reaction medium diluted with D₂O by the relative integration of the ethylene glycol protons and the acrylate protons of the PEGDMA. 0.5 M KH₂PO₄ was added in each sample to terminate the thiol-Michael addition.

2.1.5. AFM measurements

All samples were obtained by irradiating polymer precursors with green LED at intensity of 100 mW/cm² for 16 min before the tests. An atomic force microscope (Agilent 5400) was used to measure the elastic moduli of hydrogel samples. For each sample, 12–20 indentation measurements were collected. All measurements were carried out in phosphate buffered saline (PBS). The gels were indented with a pyramid-tipped probe (nanoworld, PNP-TR-20) with cantilever spring constants of 0.125 N m⁻¹, as measured by thermal calibration. Elastic moduli of the gels were calculated from force-displacement curves using a Hertz model (Carl and Schillers, 2008).

2.2. Theoretical model

Based on Bowman's network model, a network model was proposed by incorporating photobleaching and thiol-Michael addition (Reddy et al., 2006). The model consists of three parts, representing photobleaching, photopolymerization and thiol-Michael addition, respectively (represented by circles in different colors in Fig. 1). The kinetic model and derived rate equations will be introduced in Section 2.2.1, and recursive analysis in Section 2.2.2.

In the model, $[x]_0$ and $[x]_t$ denote the concentration of reactant x at

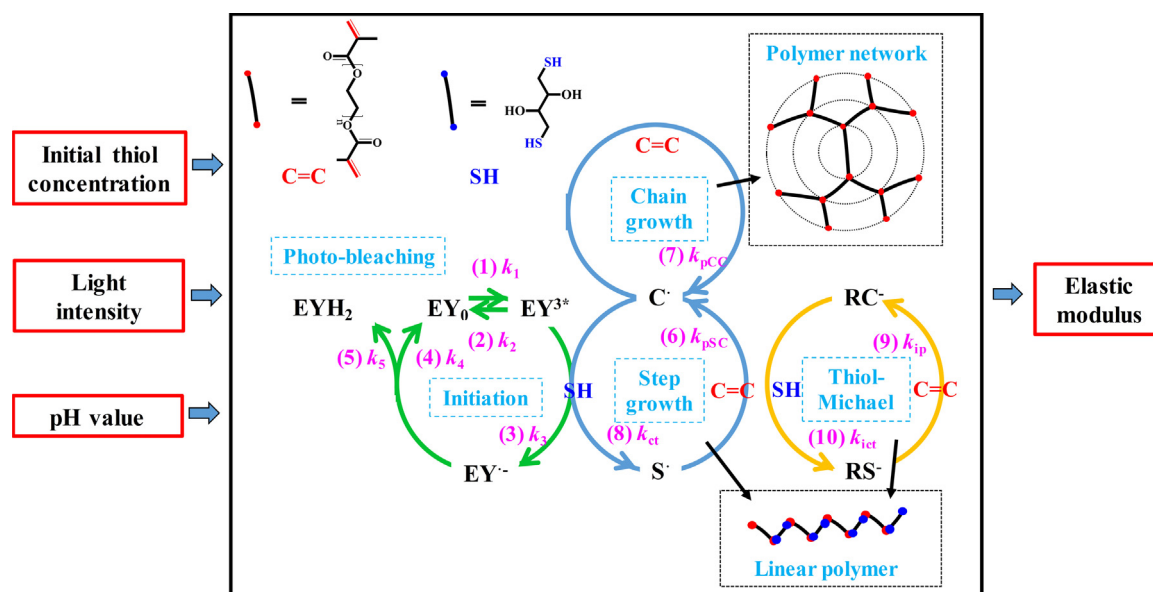


Fig. 1. Schematic of eosin Y initiated thiol-acrylate polymerization in aqueous solution. Three key factors (thiol-concentration, light intensity, pH) determine the kinetics and network development. Both photopolymerization and thiol-Michael addition were considered. SH and C=C are thiol and acrylate functional groups on DTT and PEGDMA, respectively. S[•] and C[•] are thiyl and acrylate radicals, respectively. RS⁻ and RC⁻ are thiolate anion and carbanion, respectively. EY₀ is the ground state of eosin Y, EY^{3*} is the triplet excitation state of eosin Y, EY^{•-} is the reductive radical of eosin Y, and EYH₂ is the leuco-products of eosin Y. The chain growth in photopolymerization can lead to branched polymers, a key factor determines the sol-gel transition and final elastic modulus.

initial and reaction time t , respectively, where x could be initiator, monomers, radicals or anions. $X_x(t)$ and $P_x(t)$ denote fractional concentrations and conversion, respectively, of reactant x at time t , where $x = CC, SH, EY$ for acrylate, thiol, and eosin Y, respectively. These are calculated by:

$$X_x(t) = \frac{[x]_t}{[x]_0} \quad (1)$$

$$P_x(t) = 1 - X_x(t) = 1 - \frac{[x]_t}{[x]_0} \quad (2)$$

2.2.1. Kinetic model

2.2.1.1. Photobleaching. A simple kinetic model was established according to the reported reductive electron transfer process from electron donors to eosin Y (Encinas et al., 2009; Gorner, 2008) (Fig. 1, **Process (1–5)**). Briefly, when excited by photons, eosin Y transfers to the singlet state and then relaxes to the triplet state (EY^{3*}) quickly (**Process 1**). Then, triplet eosin Y could be quenched by emitting phosphorescence and quenching by oxygen (**Process 2**) or generate reductive radicals (EY^{•-}) by reacting with various organic compounds (**Process 3**) (Grossweiner and Zwicker, 1961). The reductive radical of eosin Y could be quenched by O₂ (**Process 4**) or change into leuco-products (EYH₂) (**Process 5**). According to the scheme, the rate equations in the model could be listed as:

$$\frac{d[EY_0]_t}{dt} = -k_1[EY]_t + k_2[EY^{3*}]_t + k_4[EY^{•-}]_t \quad (3)$$

$$\frac{d[EY^{3*}]_t}{dt} = -(k_2 + k_3)[EY^{3*}]_t + k_1[EY_0]_t \quad (4)$$

$$\frac{d[EY^{•-}]_t}{dt} = -(k_4 + k_5)[EY^{•-}]_t + k_3[EY^{3*}]_t \quad (5)$$

$$\frac{d[EYH_2]_t}{dt} = k_5[EY^{•-}]_t \quad (6)$$

$$[EY_0]_t + [EY^{3*}]_t + [EY^{•-}]_t + [EYH_2]_t = 1 \quad (7)$$

where k_i ($i = 0-5$) are kinetic constants of process i (Fig. 1). k_1 is the

pump kinetic constant of triplet state (singlet state is omitted as a intermediated state), which could be calculated by $k_1 = \frac{\sigma I_{ex}}{h\nu}$, where σ is absorption section of ground state, I_{ex} is excitation light intensity, h is Planck's constant, and ν is the frequency of the excitation light (Penzkofer and Beidoun, 1993). k_2 is the relaxation rate of triplet state of eosin Y (Penzkofer and Beidoun, 1993). k_3 is the kinetic constant of reductive electron transfer, which generates anion radicals of eosin Y. This incorporates electron transfer from triplet eosin Y to thiol function groups and is related to concentration of thiols as $k_3 = k_{etSH}[SH]_t + k_{et0}$, where k_{etSH} is the reductive electron transfer rate constant of thiol groups, and k_{et0} is the reductive electron transfer rate constant of other species, which incorporates self-quenching of eosin Y and electron transfer to PEGDMA (Gorner, 2008). Note that quenching of one eosin Y in the triplet state generates less than one thiol radical, and that the number of thiol radical generated by one eosin Y in triplet state could be depicted by radical quantum yield (ϕ_R) (Arbeloa et al., 2016). Thus, the rate of generating thiol radicals by photoinitiation could be calculated by $(d[S^{\bullet-}]/dt)_{initiation} = \phi_R \cdot k_{etSH} [EY^{3*}]_t [SH]_t$. k_4 is the kinetic constant of relaxation of eosin Y from anion radical state to ground state, which could occur through oxygen scavenging (Gorner, 2008). k_5 is the kinetic constant of generation of leuco-products (Gorner, 2008). Values of these constants are listed in Table 1.

2.2.1.2. Thiol-acrylate photopolymerization. The process of thiol-acrylate photopolymerization is shown in Fig. 1. Briefly, excited eosins absorb a hydrogen from a thiol functionality, generating a thiyl radical (**Process 3**). Then the thiyl radical can propagate to an acrylate functionality and generate an acrylate radical (**Process 6**) with a kinetic constant of k_{psc} . Thereafter, the acrylate radical can either propagate to new acrylate functionality (**Process 7**) or chain transfer to a thiol functionality (**Process 8**) with kinetic constants of k_{pcc} and k_{ct} , respectively. All radicals are assumed to be terminated by combination with a kinetic constant k_t . Values of these constants are listed in Table 1

2.2.1.3. Thiol-Michael addition. The process of thiol-Michael addition between thiols and acrylates is shown in Fig. 1. Briefly, thiolate anions are generated by dynamic equilibrium between thiol functionality and

Table 1
Parameters used in the model.

Notations	Meanings	Value	Unit	Ref.
f_{CC}	Number of acrylate functionalities on PEGDMA	2	–	–
f_{SH}	Number of thiol functionalities on DTT	2	–	–
k_2	Relaxation rate of triplet state of eosin Y	$4 \cdot 10^5$	s^{-1}	(Gorner, 2008)
k_4	Kinetic constant of relaxation from anion radical state to ground state of eosin Y	$3 \cdot 10^4$	s^{-1}	(Gorner, 2008)
k_5	Kinetic constant of generation of leuco-products by eosin Y anion radical	$4.8 \cdot 10^1$	s^{-1}	estimated ^a
σ	The absorption across section of ground state of eosin Y	$3.8 \cdot 10^{-17}$	cm^2	(Penzkofer and Beidoun, 1993)
ν	The peak frequency of emission spectrum of LED	$5.77 \cdot 10^{-14}$	s^{-1}	measured ^b
k_{etSH}	Electron transfer rate constant to SH	$3.3 \cdot 10^8$	$M^{-1} s^{-1}$	(Gorner, 2008; Islam et al., 1998)
k_{etO}	Electron transfer rate constant to other molecules	$1 \cdot 10^5$	s^{-1}	estimated ^a
ϕ_R	Radical quantum yield of triplet state of eosin Y	0.06	–	(Arbeloa et al., 2016)
k_{pSC}	Kinetic constant of thiy radical propagation	$7.5 \cdot 10^3$	$M^{-1} s^{-1}$	estimated ^a
k_{pCC}	Kinetic constant of acrylate radical propagation	$3 \cdot 10^3$	$M^{-1} s^{-1}$	estimated ^a
k_{ct}	Kinetic constant of radical chain transfer	$5 \cdot 10^3$	$M^{-1} s^{-1}$	estimated ^a
k_t	Kinetic constant of radical termination	$3 \cdot 10^7$	$M^{-1} s^{-1}$	estimated ^a
k_{dp}	Kinetic constant of deprotonation of thiol functionality	1	$M^{-1} s^{-1}$	estimated ^a
k_{rdp}	Kinetic constant of reverse deprotonation of thiol functionality	408	$M^{-1} s^{-1}$	estimated ^a
k_{ip}	Kinetic constant of ionic propagation	0.14	$M^{-1} s^{-1}$	(Claudino et al., 2016)
k_{ict}	Kinetic constant of ionic chain transfer	0.96	$M^{-1} s^{-1}$	(Claudino et al., 2016)
K	Elasticity-network constant	568	$kPa M^{-1}$	estimated ^a

^a Values estimated by fitting experimental data.

^b The emission spectrum of LED is measured by QuantaMasterTM40 spectrofluorometer.

phosphate. The equilibrium constant is determined by the difference in acidities between thiol and $H_2PO_4^-$ ($\Delta pK_a = pK_{a(SH)} - pK_{a(H_2PO_4^-)}$), which follows (Claudino et al., 2016):

$$K_{eq} = \frac{k_{dp}}{k_{rdp}} = \frac{[RS^-]_t [H_2PO_4^-]_t}{[SH]_t [HPO_4^{2-}]_t} = 10^{\Delta pK_a} \quad (8)$$

where k_{dp} is the kinetic constant of deprotonation of thiol functionality, and k_{rdp} is the kinetic constant of reverse deprotonation of thiol functionality. Then, a thiolate anion can generate carbanion by anionic propagation to an acrylate functionality (**Process 9**), with a kinetic constant of k_{ip} . Carbanions are transferred back to thiol functionalities by anionic chain transfer (**Process 10**) with a kinetic constant of k_{ict} . Values of these constants are listed in Table 1.

Based on processes described above, the rate equations could be written as:

$$\begin{aligned} \frac{d[SH]_t}{dt} = & -(\phi_R \cdot k_{etSH} [EY^{3*}]_t + k_{ct} [C^*]_t + k_{ict} [RC^-]_t \\ & + k_{dp} [HPO_4^{2-}]_t) [SH]_t \\ & + k_{rdp} [H_2PO_4^-]_t [RS^-]_t \end{aligned} \quad (9)$$

$$\frac{d[CC]_t}{dt} = -(k_{pSC} [S^*]_t + k_{pCC} [C^*]_t + k_{ip} [S^-]_t) [CC]_t \quad (10)$$

$$\begin{aligned} \frac{d[RS^-]_t}{dt} = & (k_{dp} [HPO_4^{2-}]_t + k_{ict} [C^-]_t) [SH]_t \\ & - (k_{rdp} [H_2PO_4^-]_t + k_{ip} [CC]_t) [RS^-]_t \end{aligned} \quad (11)$$

$$\frac{d[RC^-]_t}{dt} = k_{ip} [CC]_t [RS^-]_t - (k_{ict} [SH]_t + k_{ict2} [H_2PO_4^-]_t) [RC^-]_t \quad (12)$$

$$\begin{aligned} \frac{d[HPO_4^{2-}]_t}{dt} = & -k_{dp} [HPO_4^{2-}]_t [SH]_t + (k_{rdp} [RS^-]_t + k_{ict2} [RC^-]_t) [H_2PO_4^-]_t \end{aligned} \quad (13)$$

$$\frac{d[H_2PO_4^-]_t}{dt} = -\frac{d[HPO_4^{2-}]_t}{dt} \quad (14)$$

$$\begin{aligned} \frac{d[S^*]_t}{dt} = & (\phi_R \cdot k_{etSH} [EY^{3*}]_t + k_{ct} [C^*]_t) [SH]_t \\ & - k_{pSC} [CC]_t [S^*]_t - k_t (2[S^*]_t + [C^*]_t) [S^*]_t \end{aligned} \quad (15)$$

$$\begin{aligned} \frac{d[C^*]_t}{dt} = & k_{pSC} [CC]_t [S^*]_t - k_{ct} [SH]_t [C^*]_t \\ & - k_t ([S^*]_t + 2[C^*]_t) [C^*]_t \end{aligned} \quad (16)$$

2.2.2. Network development analysis

Bowman's recursive modeling approach was employed to analyze the process of network development (Reddy et al., 2006). Briefly, for a defined kinetic chain, the polymerization was divided into two directions: the down direction (radical quenched on the chain) and the up direction (radical generated on the chain). Step growth and chain growth on the kinetic chain were depicted by a set of probability parameters. A step growth process terminates one arm of acrylate functionality, thus making the chain length on the pathway finite, while a chain growth process does not terminate the pathway. Through calculation of these probability parameters of kinetic chains, the possibility of finding finite kinetic chains can be obtained by recursive methods.

There are four pathways for a single di-methacrylate monomers and two pathways for a single di-thiol monomer. The monomers with i ($i = 3, 4$) pathways are considered as effective crosslinks, which determines the final elasticity of hydrogels. Thus the effective crosslinking could be obtained only by chain growth, rather than by step growth. Here, by incorporation of thiol-Michael addition, the rate of step growth is enhanced, thus probability parameters are also changed. Therefore, the modification of these parameters could be listed as followings:

(1) For the down direction,

The probability of propagation for S^* or RS^- on the kinetic chain is:

$$a_1 = \frac{(k_{pSC} [S^*]_t + k_{ip} [S^-]_t) [CC]_t}{(k_{pSC} [S^*]_t + k_{ip} [S^-]_t) [CC]_t + T_5} \quad (17)$$

where $T_5 = k_t (2[S^*]_t + [C^*]_t) [S^*]_t$ is the termination rate.

The probability of termination for S^* on the kinetic chain is:

$$a_2 = 1 - a_1 \quad (18)$$

The probability of propagation for C^* or RC^- on the kinetic chain is:

$$q_1 = \frac{k_{pCC} [C^*]_t [CC]_t}{k_{pCC} [C^*]_t [CC]_t + (k_{ct} [C^*]_t + k_{ict} [C^-]_t) [SH]_t + T_c} \quad (19)$$

where $T_C = k_t([S^*]_t + 2[C^*]_t)[C^*]_t$.

The probability of chain transfer of C^* or RC^- on the kinetic chain is:

$$q_2 = \frac{(k_{ct}[C^*]_t + k_{ict}[C^-]_t)[SH]_t}{k_{pCC}[C^*]_t[CC]_t + (k_{ct}[C^*]_t + k_{ict}[C^-]_t)[SH]_t + T_C} \quad (20)$$

The probability of termination of C^* on the kinetic chain is:

$$q_3 = 1 - q_1 - q_2 \quad (21)$$

(2) For the up direction,

The probability of pendant CC groups on the kinetic chain consumed through S^* or S^- is:

$$t_1 = \frac{(k_{psc}[S^*]_t + k_{ip}[S^-]_t)[CC]_t}{k_{pCC}[C^*]_t[CC]_t + (k_{psc}[S^*]_t + k_{ip}[S^-]_t)[CC]_t} \quad (22)$$

The probability of pendant CC groups on the kinetic chain consumed through C^* is:

$$t_2 = 1 - t_1 \quad (23)$$

The concentration of effective network chain at time t (η_t) is calculated by (Good et al., 2007):

$$\eta_t = \sum_{m=3}^{2f_{CC}} \frac{m-2}{2} [CL_m]_t \quad (24)$$

where $[CL_m]_t$ is the concentration of crosslinks with m path reaching infinite at time t .

Then the elastic modulus can be calculated by Good et al. (2007):

$$E_t = K\eta_t \quad (25)$$

where K is a constant depicting the relationship between elastic modulus and concentration of the effective network chain, which is termed as the elasticity-network constant here.

Because step growth provides negligible contribution to gelation, the criteria of gelation is determined by calculating acrylate conversion by chain growth. According to the Flory-Stockmayer equation, the gel point is approached when (Flory, 1941):

$$P_{CC, crit} |_{Chain\ growth} = P_{CC, crit} - r_0 P_{SH, crit} = \frac{1}{2f_{CC} - 1} \quad (26)$$

where $P_{CC, crit}$, $P_{CC, crit} |_{Chain\ growth}$ and $P_{SH, crit}$ are acrylate conversion, acrylate conversion by chain growth, thiol conversion at gel point respectively; f_{CC} is the number of acrylate functionalities on PEGDMA; r_0 is initial reaction stoichiometry, which is defined as $r_0 = [SH]_0/[CC]_0$. The elastic modulus at gel point is defined as E_{crit} .

The termination time (T) is defined as the time when $X_{CC}(t)$, $X_{SH}(t)$, or $X_{EY}(t) < 0.001$, the final conversion of reactant x is defined as $P_x(t)$, and the final elastic modulus of hydrogel network is defined as E_T .

The acrylate conversion rate, R_p (s^{-1}), is defined as (Iedema et al., 2018):

$$R_p = \frac{1}{1 - P_{CC, t}} \frac{dP_{CC, t}}{dt} = k_{psc}[S^*] + k_{pCC}[C^*] + k_{ip}[C^-] \quad (27)$$

where its maximum value in one polymerization process is defined as R_{pmax} .

To compare acrylate conversion with chain growth and step growth, the degree ratio of chain growth (κ_{CG}) is defined as:

$$\kappa_{CG} = \frac{P_{CC, t} |_{Chain\ growth}}{P_{CC, t}} = \frac{P_{CC, t} - r_0 P_{SH, t}}{P_{CC, t}} \quad (28)$$

where its value at termination time is defined as $\kappa_{CG, T}$.

All rate equations (Eqs. (3)–(16)) were solved by Euler's method. The simulation time period was 60,000 s and the calculation time step was 10 μs . Numerical computations were performed in MATLAB.

3. Results and discussion

To explore the role of photobleaching and thiol-Michael addition in thiol-acrylate photopolymerization, a network model was established based on combined kinetic and recursive modeling approaches. After validating with experimental results, the model was further applied to study the roles of three factors (e.g., thiol concentration, light intensity, and pH values) on the development and the final elasticity of polymer networks formed by thiol-acrylate photopolymerization. The results show that photobleaching and thiol-Michael addition can be optimized to tune thiol-acrylate photopolymerization at certain conditions, and our model provides a detailed explanation of the effects of initial thiol concentration, light intensity and pH values on the thiol-acrylate photopolymerization.

3.1. Modeling and verification of photobleaching process

To test whether the model could describe the photobleaching process, the temporal evolution of normalized eosin Y concentration (X_{EY})

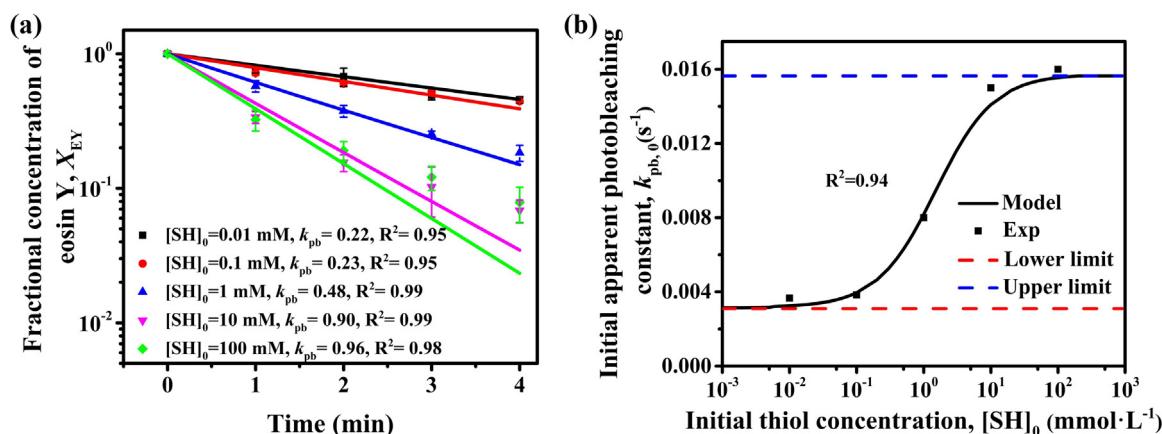


Fig. 2. Comparison of experimental data with simulation results on eosin Y consumption during photobleaching. (a) Time evolution of fractional concentration of eosin Y in precursor solution at five different thiol concentrations ($I_{ex} = 100 \text{ mW cm}^{-2}$, $[CC]_0 = 0.2 \text{ M}$). The symbols represent experimental data, and the lines represent single-exponential fits to the experimental data. Standard deviations from three independent repeated measurements are shown. (b) Kinetic constants obtained from experimental data (symbols), and model prediction (line) at different thiol concentrations. The dashed lines in red and blue color represent lower limit and upper limit of $k_{pb, 0}$ respectively.

was measured at various thiol concentrations (Fig. 2a). Results show that the concentration of eosin Y decreased with increasing time duration following a single-exponential function at in the initial stages of the reactions. Then the experimental data was fitted by a function $X_{EY} = \exp(-k_{pb, 0}t)$, and obtained the initial apparent photobleaching constant ($k_{pb, 0}$) at various thiol concentrations (Fig. 2b). The relationship between $k_{pb, 0}$ and the logarithm of initial thiol concentrations showed a sigmoidal shape, in accordance with the modeling results (Fig. 2b). This indicates that the model could capture the sigmoidal relationship between photobleaching constants and initial thiol concentrations.

To explore the mechanisms underlying the ways that thiol concentration determines photobleaching constants, a simple equation derivation was made beginning with the exponential relationship $X_{EY} = \exp(-k_{pb, 0}t)$. The concentration of leuco-products is $[EYH_2]_t = 1 - \exp(-k_{pb, 0}t)$. Substituting $[EYH_2]_t$ in Eqs. (4)–(7) with this equation generates $[EY_0]_t$, $[EY^{3*}]_t$, $[EY^{*-}]_t \propto \exp(-k_{pb, 0}t)$. Thus:

$$[EY^-]_t = \frac{k_{pb, 0}}{k_5} \exp(-k_{pb, 0}t) \quad (29)$$

$$[EY^{3*}]_t = \frac{k_4 + k_5 - k_{pb, 0}}{k_3} [EY^-]_t = \frac{k_4 + k_5 - k_{pb, 0}}{k_3} \frac{k_{pb, 0}}{k_5} \exp(-k_{pb, 0}t) \quad (30)$$

$$[EY_0]_t = \frac{k_2 + k_3 - k_{pb, 0}}{k_1} [EY^{3*}]_t = \frac{k_2 + k_3 - k_{pb, 0}}{k_1} \frac{k_4 + k_5 - k_{pb, 0}}{k_3} \frac{k_{pb, 0}}{k_5} \exp(-k_{pb, 0}t) \quad (31)$$

$$(k_1 - k_{pb, 0})[EY_0]_t = k_2[EY^{3*}]_t + k_4[EY^{*-}]_t \quad (32)$$

Eliminating the terms of reactant concentrations in Eqs. (29)–(32), the following relationship could be obtained:

$$\frac{k_5 - k_{pb, 0}}{k_4 + k_5 - k_{pb, 0}} \frac{k_3}{k_{pb, 0}} = \frac{k_1 + k_2 + k_3 - k_{pb, 0}}{k_1} \quad (33)$$

From Table 1 and Fig. 2b, $k_{pb, 0} \ll k_i$, and $k_1 \ll k_2$. Then, the relationship between $k_{pb, 0}$ and $[SH]_0$ could be obtained from Eq. (33):

$$k_{pb, 0} \approx \frac{k_3}{k_1 + k_2 + k_3} \frac{k_1 k_5}{k_4 + k_5} \approx \frac{k_{et0} + k_{etSH} [SH]_0}{k_2 + k_{et0} + k_{etSH} [SH]_0} \frac{k_5}{k_4 + k_5} \frac{\sigma I_{ex}}{h\nu} \quad (34)$$

From this, the sigmoidal shape could be depicted by a simplified equation (Eq. (34)), and that there are two limits of $k_{pb, 0}$, namely

$$k_{pb, 0}^{lower\ limit} = \frac{k_{et0}}{k_2 + k_{et0}} \frac{k_1 k_5}{k_4 + k_5} \quad \text{when} \quad [SH]_0 \rightarrow 0, \quad \text{and}$$

$$k_{pb, 0}^{upper\ limit} = \frac{k_1 k_5}{k_4 + k_5} \quad \text{when} \quad [SH]_0 \rightarrow \infty.$$

From Eq. (34), a general relationship between the apparent photobleaching constant of eosin Y, k_{pb} , and thiol concentration, $[SH]_t$ could be obtained:

$$k_{pb} = \frac{k_{et0} + k_{etSH} [SH]_t}{k_2 + k_{et0} + k_{etSH} [SH]_t} \frac{k_5}{k_4 + k_5} \frac{\sigma I_{ex}}{h\nu} \quad (35)$$

This relationship was used to simplify the calculation of Eqs. (3)–(7). A similar relationship between dye consumption kinetics and donor concentration and light intensity may also exist in other dye/electron donor initiation systems.

3.2. Modeling and verification of mechanical properties and acrylate conversion of thiol-acrylate hydrogels

To check whether the established model can also simulate the whole photopolymerization process, further comparison between the simulation results and experimental data was made in terms of final elastic moduli and acrylate conversion of the hydrogels (Fig. 3). The final elastic moduli (E_T) of hydrogels (irradiated for 16 min) formed at different initial thiol concentrations ($[SH]_0$) were measured using AFM

(Fig. 3a, symbols). No crosslinking could be observed when $[SH]_0$ is below 1 mM, or above 100 mM, and there exists a peak value of E_T at $[SH]_0 = 10$ mM. The model prediction of final elastic moduli is shown in Fig. 3a (line), which captures the experimentally observed trends.

Next, the final acrylate conversion ($P_{CC, T}$) formed at different initial thiol concentrations was measured using $^1\text{H NMR}$. In contrast to the up-down relationship between elastic modulus and initial thiol concentration, these results show that the final acrylate conversion increases monotonically with increasing initial thiol concentration (Fig. 3b, symbols), which is also well predicted by the modeling (Fig. 3b, line). These results demonstrate that the model is capable of predicting the elasticity and acrylate conversion of this reaction system.

3.3. Modeling and verification of thiol-Michael addition

To verify the mathematical model of thiol-Michael addition between thiols and acrylates, the temporal evolution of vinyl conversion was measured by $^1\text{H NMR}$. Eosin Y was not added in the reaction to prevent photopolymerization, and the pH was tuned to 8.3 using phosphates. Experiments were conducted using five different initial monomer concentrations (C1–C5). For C1–C3, the initial acrylate concentration increased from 0.05 to 0.2 M at a fixed initial thiol concentration of 0.05 M. For C3–C5, the initial thiol concentration increased from 0.05 to 0.2 M at a fixed initial acrylate concentration of 0.2 M. It could be observed that when the concentration of acrylate increases at a fixed thiol concentration, the overall reaction rates (C1–C3) increases, while keeping acrylate concentration constant has no obvious effect on the reaction rates (C3–C5). This indicates that $k_{ip} \gg k_{ict}$ (Claudino et al., 2016). This phenomenon is in accordance with that observed for thiol-vinyl sulfone Michael addition (Claudino et al., 2016). Thus, in this model, the same group of kinetic constants were adopted, and it shows that the simulation results fit well with experiments data (Fig. 4a).

The ionization of thiolate anions is highly dependent on the pH value. Thus, the pH value could also have notable effect on overall polymerization rate of thiol-Michael addition (Nair et al., 2014). To explore the effect of pH value on thiol-Michael addition, the time evolution process of thiol-Michael addition was calculated under four different pH values (Fig. 4b). It is found that pH value could significantly affect the overall reaction rate of thiol-Michael addition. The final thiol conversion could reach 90% after 32 min reaction in a solution with pH value of 8.3, while the final thiol conversion would reach only 9% when the pH value drops to 6.8. These results indicate that pH value could also greatly affect the kinetics of thiol-acrylate photopolymerization due to the co-existence of thiol-Michael addition.

3.4. The effect of initial thiol concentration on elastic modulus

It has been shown that there is a “parabolic relationship” between elastic modulus and initial thiol concentration for PEGDA/NVP hydrogels (Hao and Lin, 2014). However, the underlying mechanism remains elusive and this hinders the understanding the effect of initial thiol concentration on final elastic modulus. The simulation results of the developed model show that this “parabolic relationship” exists in a wide region of light intensity (1–100 mW cm⁻²), and that the maximum final elastic modulus could be obtained at $[SH]_0 = 10$ mM (Fig. 5a). When initial thiol concentration varies from 1 to 100 mM, the ratio of the maximum and minimum final elastic modulus reach 1.63, 1.93, 1.62 at $I_{ex} = 1, 10, 100$ mW cm⁻² respectively. This suggests that initial thiol concentration affects the final elastic modulus.

To explore the mechanism underlying these “parabolic” relationships, maximum acrylate conversion rate (R_{pmax}) (Fig. 5b) and final degree of chain growth ($\kappa_{CG, T}$) (Fig. 5c) were simulated with varying initial thiol concentration at different light intensities from 1 to 100 mW cm⁻². It is found that with increasing initial thiol concentration from 1 to 100 mM, R_{pmax} increases nearly linearly, while $\kappa_{CG, T}$ exhibits

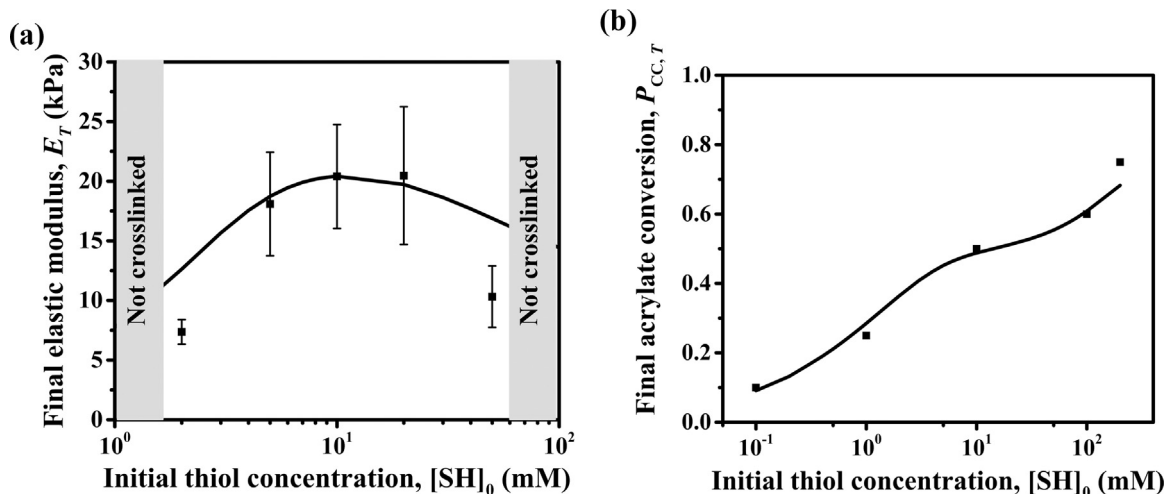


Fig. 3. Comparison of experimental data and simulation estimates of final elastic moduli of and acrylate conversion in thiol-acrylate hydrogels. (a) Experimental characterization (symbols) and model prediction (line) of the final elastic moduli of hydrogels (E_T) at different initial thiol concentrations. (b) Experimental characterization (symbols) and model prediction (line) of the final acrylate conversion ($P_{CC,T}$) at different thiol concentrations. The gray areas (thiol concentration below 2 mM or above 500 mM) in (a) indicate no gel formation. All experimental data were obtained from samples irradiated for 16 min ($I_{ex} = 100 \text{ mW cm}^{-2}$, $[CC]_0 = 0.2 \text{ M}$, $\text{pH} = 6.8$).

an accelerating declining process under a certain light intensity. Thus, it could be concluded that final elastic modulus increases with increasing initial thiol concentration due to increased gelation kinetics, while the modulus decreases with further increase in thiol concentration due to decreased degree of chain growth.

Fig. 5d shows the dependence of elastic modulus on acrylate conversion with varying initial thiol concentration at light intensity of 1 mW cm^{-2} . With increasing initial thiol concentration increases from 0.1 to 100 mM, the final acrylate conversion rises from 46.0% to 98.4%, while the gel point is also reached at a higher acrylate conversion value (from 33.4% to 63.9%). It could also be observed that, despite the large variation (23.9–93.3 kPa) of final elastic modulus (E_T) at different initial thiol concentration, the elastic modulus at gel point (E_{crit}) is relatively close (11.0–16.4 kPa).

3.5. The effect of light intensity on elastic modulus

To explore the effect of light intensity on final elastic modulus, the

temporal evolution of elastic modulus was simulated at various light intensities (from 1 to 100 mW cm^{-2}) with a fixed initial thiol concentration of 10 mM (Fig. 6). With increasing light intensity, the gel point shortens from 904 s to 147 s, while the final elastic modulus decreases from 93.3 kPa to 20.4 kPa (Fig. 6a). Evaluating the effect of light intensity on eosin Y conversion as a function of time (Fig. 6b) reveals that with increasing light intensity, the consumption of eosin Y accelerates due to the linear relationship between apparent photobleaching rate constant (k_{pb}) and light intensity (I_{ex}) (cf. Eq. (35)). Due to this accelerated eosin Y consumption at increased light intensity, acrylate conversion decreases, resulting in decreased elastic modulus (Fig. 6c). With increasing light intensity, normalized acrylate conversion rate, R_p/R_{pmax} declines rapidly with eosin Y conversion (Fig. 6d). These results indicate that eosin Y possesses higher initiation efficiency at a lower light intensity, which contributes to a higher final elastic modulus.

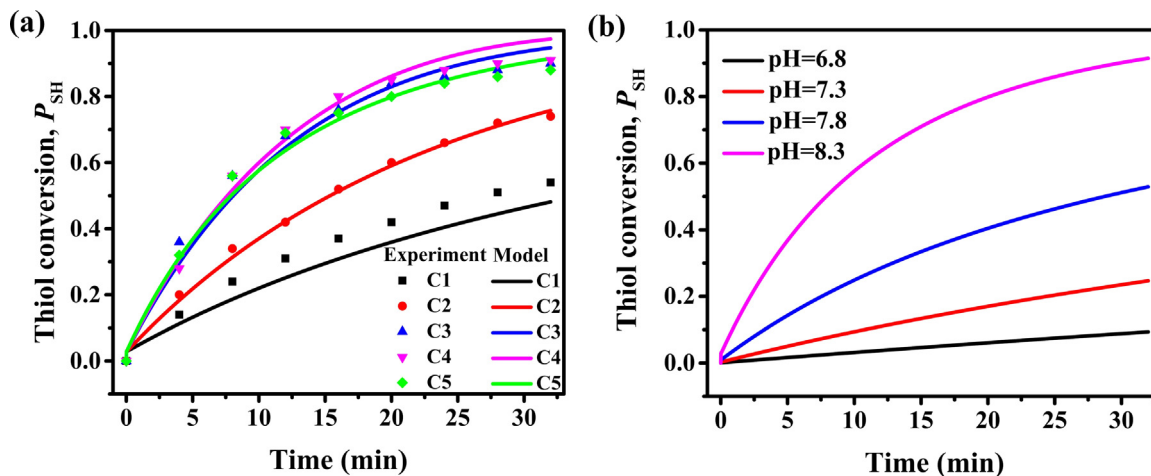


Fig. 4. Comparison of experimental results and simulation predictions of thiol conversion by thiol-Michael addition. (a) Experimental characterization of temporal evolution of thiol conversion by thiol-Michael addition (symbols) and model predictions (lines) under different initial monomer concentrations at $\text{pH} = 8.3$. The groups C1–C5 are referred as C1: $[CC]_0 = 0.05 \text{ M}$, $[SH]_0 = 0.05 \text{ M}$; C2: $[CC]_0 = 0.1 \text{ M}$, $[SH]_0 = 0.05 \text{ M}$; C3: $[CC]_0 = 0.2 \text{ M}$, $[SH]_0 = 0.05 \text{ M}$; C4: $[CC]_0 = 0.2 \text{ M}$, $[SH]_0 = 0.1 \text{ M}$; C5: $[CC]_0 = 0.2 \text{ M}$, $[SH]_0 = 0.2 \text{ M}$. (b) Model prediction of temporal evolution of thiol conversion by thiol-Michael addition under different pH values (6.8–8.3).

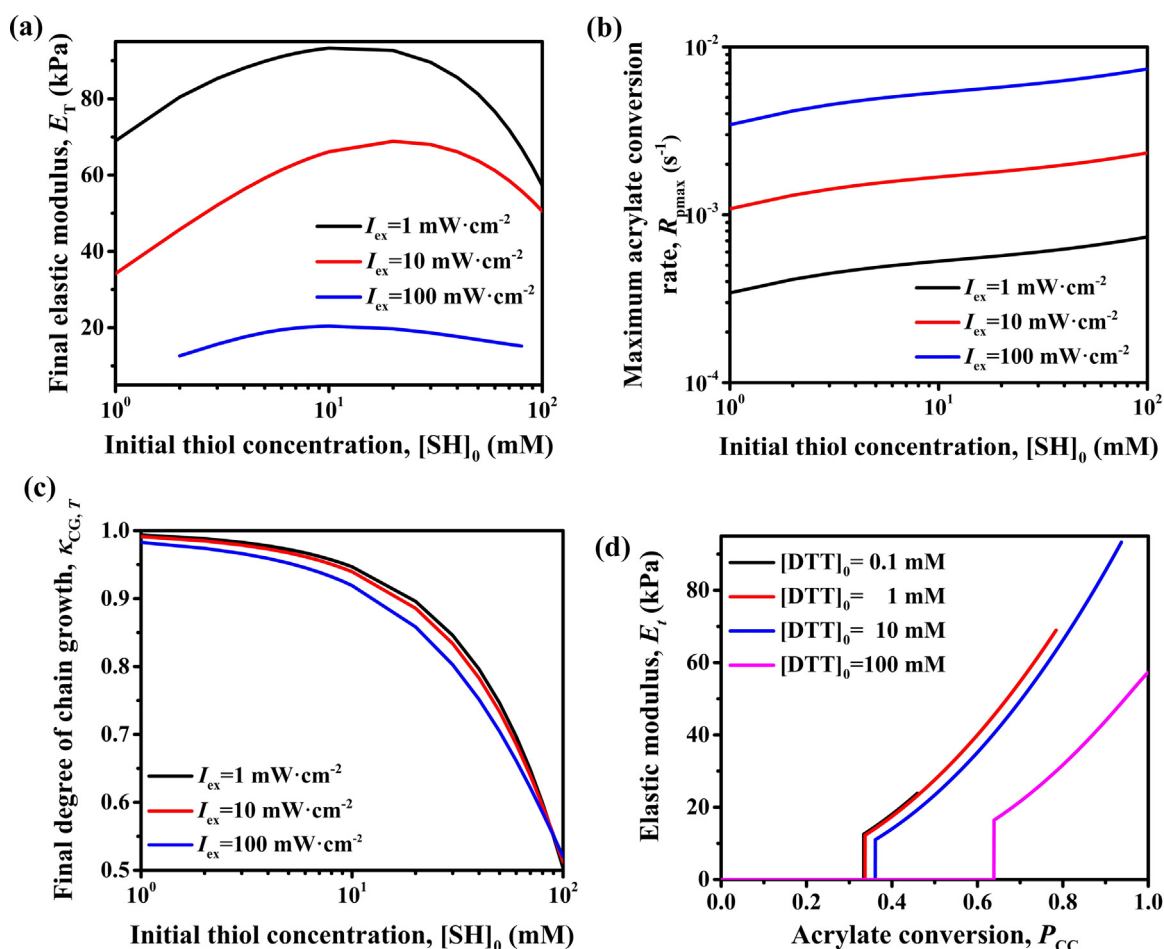


Fig. 5. Predictions of the effect of initial thiol concentrations on final elastic modulus and kinetics of network development at different light intensities (1, 10, 100 $\text{mW}\cdot\text{cm}^{-2}$), $[\text{CC}]_0 = 0.2\text{ M}$, and $\text{pH} = 6.8$. (a) Final elastic modulus as a function of initial thiol concentration at different light intensity. (b) Maximum acrylate conversion rate as a function of initial thiol concentration at different light intensity. (c) Final degree of chain growth as a function of initial thiol concentration at different light intensity. (d) Dependence of elastic modulus on acrylate conversion rate with varying initial thiol concentration at light intensity of $1\text{ mW}\cdot\text{cm}^{-2}$.

3.6. The effect of pH value on elastic modulus

When the thiol-acrylate photopolymerization process is considered under alkaline pH conditions, thiol-Michael addition plays an important role in determining the final elastic modulus, especially at low light intensity. To explore the effect of pH value on final elastic modulus, the final elastic modulus of hydrogels was compared by calculating the ratio of final elastic modulus of hydrogels formed in neutral and alkaline solution ($E_T(\text{pH} = 8.3)/E_T(\text{pH} = 6.8)$) at different light intensity and thiol concentration (Fig. 7). It is found that when thiol concentration is below 10 mM or light intensity is below $10\text{ mW}\cdot\text{cm}^{-2}$, gels formed in alkaline solution are more compliant than those formed in neutral solution. With decreasing thiol concentration or light intensity, this softening effect by increasing pH value becomes more effective. This phenomenon is mainly due to the increased degree of step growth caused by competition of thiol-Michael addition. Due to the nature of thiol-Michael addition (Claudino et al., 2016), it could be deduced that when the light intensity is low enough, the increased linear addition by thiol-Michael addition will limit the production of branched polymers, and prevent the occurrence of gelation. By capturing this phenomenon, the model could simulate some conditions which could haven't been considered by existed thiol-ene photopolymerization models (Derboven et al., 2013; Lee et al., 2007; Reddy et al., 2006).

4. Conclusions

A network model that couples kinetic and recursive approaches has been developed to predict elastic modulus of hydrogels formed by eosin Y initiated thiol-acrylate photopolymerization. By incorporating photobleaching of eosin Y and thiol-Michael addition processes, the model simulations show good accordance with experimental results. The simulation results indicate that the initial thiol concentration, light intensity and pH value play important roles in determining the final elastic moduli of hydrogels through controlling kinetics of chain growth and step growth.

The developed model shows that the optimal initial thiol concentration for 0.2 M PEGDMA is 10 mM, which is invariant for light intensity over the range of 1–100 $\text{mW}\cdot\text{cm}^{-2}$. Modeling results also predict that decreasing the light intensity can increase the final elastic modulus by improving initiation efficiency of eosin Y. Finally, the simulation results support that thiol-Michael addition plays an important role in determining the final elastic modulus of hydrogel formed in alkaline solution, when light intensity or initial thiol concentration is low enough. For this latter effect, the model reveals a new kinetic pathway, namely that thiol-Michael addition consumes acrylate monomers without light irradiation, thereby inhibiting gelation and limiting the storage time of precursors.

Taken together, the results show that the developed model has the capacity to enable optimized hydrogel reaction kinetics for finely tuned

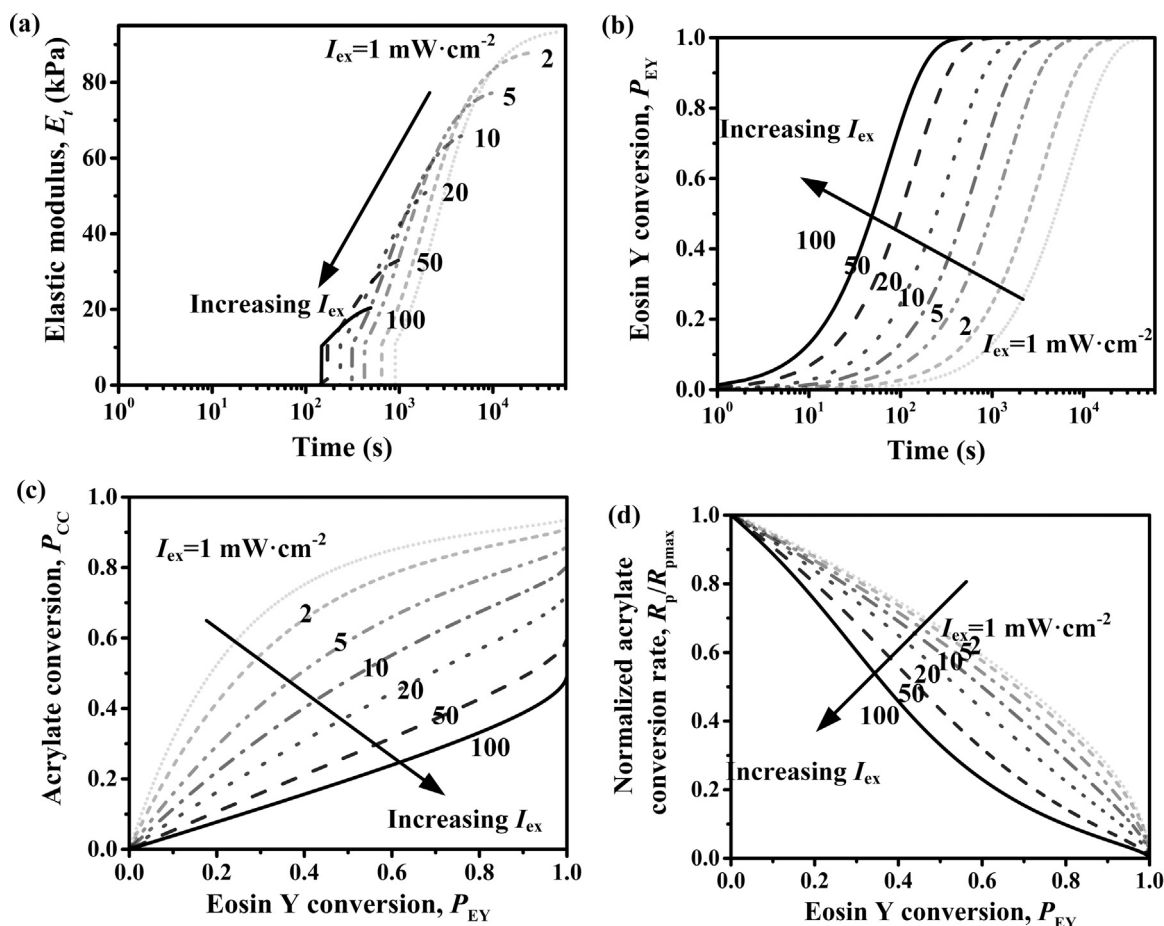


Fig. 6. Predictions of the effect of light intensity on kinetic profiles at $[SH]_0 = 10 \text{ mM}$, $[CC]_0 = 0.2 \text{ M}$ pH = 6.8. (a) Effect of light intensity on elastic modulus as a function of time. (b) Effect of light intensity on eosin Y conversion as a function of time. (c) Effect of light intensity on acrylate conversion as a function of eosin Y conversion. (d) Effect of light intensity on normalized acrylate conversion rate (R_p/R_{pmax}) as a function of eosin Y conversion.

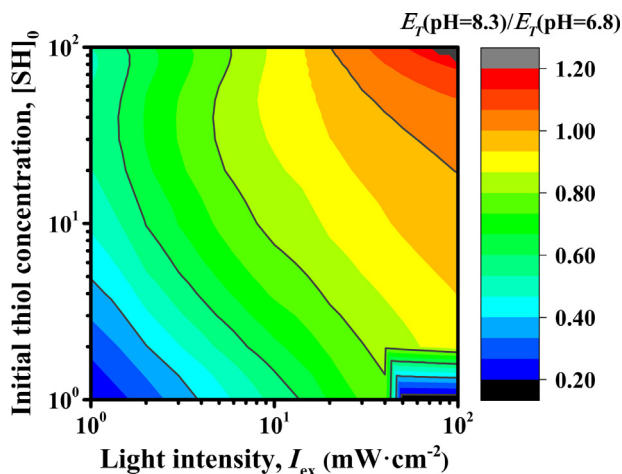


Fig. 7. Predictions of the effect of pH on the final elastic modulus of hydrogels. Contours show the ratio between predicted elastic moduli of gels formed in neutral and alkaline solution ($E_t(\text{pH} = 8.3)/E_t(\text{pH} = 6.8)$) at different light intensity (1–100 mW/cm^2) and initial thiol concentration (1–100 mM), with $[CC]_0 = 0.2$.

elastic moduli. Compared with existing models for thiol-acrylate photopolymerization, the developed model provides a more realistic prediction and a detailed understanding of elastic modulus affected by various reaction conditions.

Acknowledgements

This work was supported by the National Natural Science Foundation of China (11772253), the Natural Science Foundation of Shaanxi Province (2018JM1007), the Fundamental Research Funds for the Central Universities (2016qngz03), the NIH through Grant U01EB016422, and the NSF Center for Engineering Mechano-Biology (Grant CMMI-1548571).

References

- Arbeloa, E.M., Previtali, C.M., Bertolotti, S.G., 2016. Photochemical study of Eosin-Y with PAMAM dendrimers in aqueous solution. *J. Lumin.* 180, 369–375.
- Brown, T.E., Anseth, K.S., 2017. Spatiotemporal hydrogel biomaterials for regenerative medicine. *Chem. Soc. Rev.* 46, 6532–6552.
- Carl, P., Schillers, H., 2008. Elasticity measurement of living cells with an atomic force microscope: data acquisition and processing. *Pflug. Arch. Eur. J. Phys.* 457, 551–559.
- Cheng, B., Lin, M., Huang, G., Li, Y., Ji, B., Genin, G.M., Deshpande, V.S., Lu, T.J., Xu, F., 2017. Cellular mechanosensing of the biophysical microenvironment: a review of mathematical models of biophysical regulation of cell responses. *Phys. Life Rev.* 22–23, 88–119.
- Chung, S., Lee, H., Kim, H.-S., Kim, M.-G., Lee, L.P., Lee, J.Y., 2016. Transdermal thiol-acrylate polyethylene glycol hydrogel synthesis using near infrared light. *Nanoscale* 8, 14213–14221.
- Claudino, M., Zhang, X., Alim, M.D., Podgórski, M., Bowman, C.N., 2016. Mechanistic kinetic modeling of thiol-Michael addition photopolymerizations via photocaged “superbase” generators: an analytical approach. *Macromolecules* 49, 8061–8074.
- Cramer, N.B., Bowman, C.N., 2001. Kinetics of thiol-ene and thiol-acrylate photopolymerizations with real-time fourier transform infrared. *J. Polym. Sci. Polym. Chem.* 39, 3311–3319.
- Cramer, N.B., Reddy, S.K., O'Brien, A.K., Bowman, C.N., 2003. Thiol-ene photopolymerization mechanism and rate limiting step changes for various vinyl functional group chemistries. *Macromolecules* 36, 7964–7969.

- Dadashi-Silab, S., Doran, S., Yagci, Y., 2016. Photoinduced electron transfer reactions for macromolecular syntheses. *Chem. Rev.* 116, 10212–10275.
- Derboven, P., D'hooge, D.R., Stamenovic, M.M., Espeel, P., Marin, G.B., Du Prez, F.E., Reyniers, M.-F., 2013. Kinetic modeling of radical thiol–ene chemistry for macromolecular design: importance of side reactions and diffusional limitations. *Macromolecules* 46, 1732–1742.
- Encinas, M.V., Rufs, A.M., Bertolotti, S.G., Previtali, C.M., 2009. Xanthene dyes/amine as photoinitiators of radical polymerization: a comparative and photochemical study in aqueous medium. *Polymer* 50, 2762–2767.
- Flory, P.J., 1941. Molecular size distribution in three dimensional polymers. I. Gelation. *J. Am. Chem. Soc.* 63, 3083–3090.
- Fu, A., Gwon, K., Kim, M., Tae, G., Kornfield, J.A., 2015. Visible-light-initiated thiol–acrylate photopolymerization of heparin-based hydrogels. *Biomacromolecules* 16, 497–506.
- Good, B.T., Reddy, S., Davis, R.H., Bowman, C.N., 2007. Tailorable low modulus, reversibly deformable elastomeric thiol–ene materials for microfluidic applications. *Sens. Actuators B Chem.* 120, 473–480.
- Gomer, H., 2008. Oxygen uptake induced by electron transfer from donors to the triplet state of methylene blue and xanthene dyes in air-saturated aqueous solution. *Photochem. Photobiol. Sci.* 7, 371–376.
- Greene, T., Lin, T.-Y., Andrisani, O.M., Lin, C.-C., 2017. Comparative study of visible light polymerized gelatin hydrogels for 3D culture of hepatic progenitor cells. *J. Appl. Polym. Sci.* 134.
- Grossweiner, L.I., Zwicker, E.F., 1961. Transient measurements of photochemical processes in dyes. I. The photosensitized oxidation of phenol by eosin and related dyes. *J. Chem. Phys.* 34, 1411–1417.
- Han, F., Zhu, C., Guo, Q., Yang, H., Li, B., 2016. Cellular modulation by the elasticity of biomaterials. *J. Mater. Chem. B* 4, 9–26.
- Hao, Y., Lin, C.-C., 2014. Degradable thiol–acrylate hydrogels as tunable matrices for three-dimensional hepatic culture. *J. Biomed. Mater. Res. A* 102, 3813–3827.
- Hao, Y., Shih, H., Muñoz, Z., Kemp, A., Lin, C.-C., 2014. Visible light cured thiol–vinyl hydrogels with tunable degradation for 3D cell culture. *Acta Biomater.* 10, 104–114.
- Herculano, L.S., Malacarne, L.C., Zanuto, V.S., Lukasiewicz, G.V.B., Capeloto, O.A., Astrath, N.G.C., 2013. Investigation of the photobleaching process of eosin Y in aqueous solution by thermal lens spectroscopy. *J. Phys. Chem. B* 117, 1932–1937.
- Higham, A.K., Garber, L.A., Latschaw, D.C., Hall, C.K., Pojman, J.A., Khan, S.A., 2014. Gelation and cross-linking in multifunctional thiol and multifunctional acrylate systems involving an in situ comonomer catalyst. *Macromolecules* 47, 821–829.
- Hoyle, C.E., Bowman, C.N., 2010. Thiol–ene click chemistry. *Angew. Chem. Int. Ed.* 49, 1540–1573.
- Huang, G., Li, F., Zhao, X., Ma, Y., Li, Y., Lin, M., Jin, G., Lu, T.J., Genin, G.M., Xu, F., 2017. Functional and biomimetic materials for engineering of the three-dimensional cell microenvironment. *Chem. Rev.* 117, 12764–12850.
- Iedema, P.D., Schamböck, V., Boonen, H., Koskamp, J., Schellekens, S., Willemse, R., 2018. Photocuring of di-acrylate. *Chem. Eng. Sci.* 176, 491–502.
- Islam, S.D.-M., Yoshikawa, Y., Fujitsuka, M., Watanabe, A., Ito, O., 1998. Studies on photochemical processes of xanthene dyes by means of the transient absorption spectra in the visible/near-IR regions. *B. Chem. Soc. Jpn.* 71, 1543–1548.
- Kızıl, S., Pérez-Luna, V.H., Teymour, F., 2006. Mathematical model for surface-initiated photopolymerization of poly(ethylene glycol) diacrylate. *Macromol. Theor. Simul.* 15, 686–700.
- Kryven, I., Iedema, P.D., 2013. A novel approach to population balance modeling of reactive polymer modification leading to branching. *Macromol. Theor. Simul.* 22, 89–106.
- Kryven, I., Iedema, P.D., 2014a. Topology evolution in polymer modification. *Macromol. Theor. Simul.* 23, 7–14.
- Kryven, I., Iedema, P.D., 2014b. Transition into the gel regime for free radical cross-linking polymerisation in a batch reactor. *Polymer* 55, 3475–3489.
- Kryven, I., Iedema, P.D., 2015. Transition into the gel regime for crosslinking radical polymerisation in a continuously stirred tank reactor. *Chem. Eng. Sci.* 126, 296–308.
- Lee, T.Y., Smith, Z., Reddy, S.K., Cramer, N.B., Bowman, C.N., 2007. Thiol–allyl ether–methacrylate ternary systems. Polymerization mechanism. *Macromolecules* 40, 1466–1472.
- Lin, T.Y., Bragg, J.C., Lin, C.C., 2015. Designing visible light-cured thiol–acrylate hydrogels for studying the HIPPO pathway activation in hepatocellular carcinoma cells. *Macromol. Biosci.* 16, 496–507.
- Liu, Z., Lin, Q., Sun, Y., Liu, T., Bao, C., Li, F., Zhu, L., 2014. Spatiotemporally controllable and cytocompatible approach builds 3D cell culture matrix by photo-uncaged-thiol Michael addition reaction. *Adv. Mater.* 26, 3912–3917.
- Marklein, R.A., Burdick, J.A., 2010. Spatially controlled hydrogel mechanics to modulate stem cell interactions. *Soft Matter* 6, 136–143.
- Nair, D.P., Podgórski, M., Chatani, S., Gong, T., Xi, W., Fenoli, C.R., Bowman, C.N., 2014. The thiol–Michael addition click reaction: a powerful and widely used tool in materials chemistry. *Chem. Mater.* 26, 724–744.
- Penzkofer, A., Beidoun, A., 1993. Triplet–triplet absorption of eosin Y in methanol determined by nanosecond excimer laser excitation and picosecond light continuum probing. *Chem. Phys.* 177, 203–216.
- Popielarz, R., Vogt, O., 2008. Effect of coinitiator type on initiation efficiency of two-component photoinitiator systems based on Eosin. *J. Polym. Sci. Polym. Chem.* 46, 3519–3532.
- Rape, A.D., Zibinsky, M., Murthy, N., Kumar, S., 2015. A synthetic hydrogel for the high-throughput study of cell–ECM interactions. *Nat. Commun.* 6.
- Reddy, S.K., Okay, O., Bowman, C.N., 2006. Network development in mixed step-chain growth thiol–vinyl photopolymerizations. *Macromolecules* 39, 8832–8843.
- Ruskowitz, E.R., DeForest, C.A., 2018. Photoresponsive biomaterials for targeted drug delivery and 4D cell culture. *Nat. Rev. Mater.* 3, 17087.
- Sadtler, K., Singh, A., Wolf, M.T., Wang, X., Pardoll, D.M., Elisseeff, J.H., 2016. Design, clinical translation and immunological response of biomaterials in regenerative medicine. *Nat. Rev. Mater.* 1, 16040.
- Schamboeck, V., Kryven, I., Iedema, P.D., 2017. Acrylate network formation by free-radical polymerization modeled using random graphs. *Macromol. Theor. Simul.* 26.
- Shih, H., Lin, C.-C., 2013. Visible-light-mediated thiol–ene hydrogelation using Eosin-Y as the only photoinitiator. *Macromol. Rapid Commun.* 34, 269–273.
- Ulasan, M., Yavuz, E., Bagriacik, E.U., Cengeloglu, Y., Yavuz, M.S., 2015. Biocompatible thermoresponsive PEGMA nanoparticles crosslinked with cleavable disulfide-based crosslinker for dual drug release. *J. Biomed. Mater. Res. A* 103, 243–251.
- Wong, J., Kastrup, K., Aguirre-Soto, A., Sikes, H.D., 2015. A quantitative analysis of peroxy-mediated cyclic regeneration of eosin under oxygen-rich photopolymerization conditions. *Polymer* 69, 169–177.
- Yao, H., Wang, J., Mi, S., 2018. Photo processing for biomedical hydrogels design and functionality: a review. *Polymers* 10, 11.